A Simple and Effective Noise Whitening Method for Underwater Acoustic OFDM

Christian R. Berger, Shengli Zhou, Weian Chen, and Jie Huang Department of Electrical and Computer Engineering, University of Connecticut, Storrs, Connecticut 06269, USA

Abstract-Underwater acoustic OFDM enables simple frequency domain equalization, but its performance is often limited by intercarrier interference (ICI) that is induced by channel variation, in addition to the ambient noise. As the signal itself, the variance of the ICI is frequency dependent as i) the transmitter often has a non-ideal transmit voltage response (TVR), and ii) underwater acoustic propagation introduces frequency dependent attenuation. In this paper, we propose a simple method to account for the frequency-dependent spectrum of the ICI plus noise. Specifically, we approximate the power spectrum of the ICI plus noise by a straight line in the log-domain, by fitting the measurements on the null subcarriers embedded in each OFDM block. Prewhitening is then applied to each OFDM block before channel estimation and data demodulation. We test the proposed method using experimental data collected from the SPACE08 experiment, where we compare signals with and without transmitter precompensation side by side. The proposed method effectively improves the performance of the uncompensated transmission, making it comparable to that of the compensated transmission at short distances. At a longer distance, the performance of both transmissions is improved by noise-whitening, with an impressive gain on the uncompensated signals.

I. INTRODUCTION

Underwater acoustic (UWA) channels are wideband in nature due to the large bandwidth to carrier frequency ratio. Frequency dependency is one unique feature that distinguishes wideband from narrowband channels. Specifically, for underwater acoustic communication systems, the following facts are well known:

- The transmitter has a non-flat transmit voltage response (TVR), as perfect circuit matching to the transducer is difficult to achieve across the whole signal band.
- Signal attenuation depends on both the distance and the frequency [1]–[3]. In general, high frequency acoustic signals are absorbed more than low frequency signals.
- The noise spectrum is not white [1]–[3].

These effects, however, have rarely been incorporated into practical receiver designs.

Multicarrier modulation in the form of orthogonal frequency division multiplexing (OFDM) has been extensively investigated recently [4]–[13]. We in this paper consider the block-by-block receiver in [5], which treats the residual ICI on each subcarrier as additive noise. We aim to improve the system performance by accounting for the frequency dependent spectrum of the ICI plus noise.

This work is supported by the NSF grant CNS-0721834, the ONR grants N00014-07-1-0805 (YIP) and N00014-09-1-0704 (PECASE).

We propose a simple method based on the null subcarriers inserted in every OFDM symbol [5]. We approximate the spectrum of the ICI plus noise as a straight line in the logarithmic scale. The offset and the slope of the line are estimated on a block-by-block basis, by fitting the measurements on the null subcarriers. The receiver then prewhitens the current OFDM block before channel estimation and data demodulation.

We test the proposed method using data recorded from the SPACE08 experiment, which was conducted off the coast of Martha's Vineyard, MA, U.S., during October 2008. We conduct side-by-side performance comparisons on two sets of signals, where one signal set does not apply a digital filter to compensate the non-ideal transmitter voltage response, and the other does. We have the following observations:

- The uncompensated signals have 3-6 dB more power relative to the compensated signals. The compensation filter increases the peak-to-average-power ratio (PAPR) of the uncompensated signals. Hence, the transmitter attenuated the compensated signals more to meet the peak voltage constraint.
- At the distances of 60 m and 200 m, the spectrum of the compensated signals is approximately white, while that of the uncompensated signals is heavily colored. The performance of the uncompensated signals is worse than that of the compensated signals, when the colored noise is neglected. When the proposed method is applied, considerable performance improvement is observed on the uncompensated signals, leading to a comparable performance with that of the compensated signals. These results show that the receiver is operating at an ICIlimited scenario.
- At the distance of 1,000 m, both uncompensated and compensated signals show strong attenuation at high frequencies. The proposed method effectively improves the performance for both sets of signals. The uncompensated signals now have better performance than the compensated signals do, due to the higher transmit power, indicating that the noise effect shows up in addition to the ICI effect.

The rest of this paper is organized as follows. Section II describes the system model and Section III presents the proposed noise-whitening method. Performance evaluation is carried out in Section IV based on experimental data and concluding remarks are collected in Section V.

II. SYSTEM MODEL

When describing the system model, we highlight the frequency dependency at the transmitter, the channel, and the receiver.

A. Transmitter voltage response

We consider zero-padded (ZP) OFDM as in [4], [5]. Let T denote the signal duration and T_g the zero padding interval, leading to a total OFDM block duration of $T' = T + T_g$. The subcarriers are located at frequencies

$$f_k = f_c + k/T,$$
 $k = -K/2, ..., K/2 - 1,$ (1)

where f_c is the center frequency, K is the total number of subcarriers. The subcarrier spacing is 1/T and the bandwidth is B = K/T.

Define S_A and S_N as the non-overlapping sets of active and null subcarriers, respectively, that satisfy $S_A \cup S_N = \{-K/2, \ldots, K/2 - 1\}$. Let s[k] denote the symbol to be transmitted on the kth subcarrier. The designed OFDM signal in the passband is:

$$\tilde{s}(t) = 2\operatorname{Re}\left\{\sum_{k \in S_A} s[k]e^{j2\pi f_k t}g(t)\right\}, \quad t \in [0, T']. \tag{2}$$

where g(t) is the pulse shaping filter. In ZP-OFDM with rectangular pulse shaping, we have

$$g(t) = \begin{cases} 1, & t \in [0, T]; \\ 0, & \text{otherwise.} \end{cases}$$
 (3)

Other pulse shaping filters such as raised cosine filters can be considered as well. The Fourier transform of $\tilde{s}(t)$ is

$$\tilde{S}(f) = \sum_{k \in \mathcal{S}_A} s[k]G(f - f_k),\tag{4}$$

for all positive frequencies f > 0; we ignore the negative frequency part in our presentation because for any real signal $\tilde{S}(-f) = \tilde{S}^*(f)$. G(f) is the Fourier transform of g(t). For g(t) in (3), we have

$$G(f) = \frac{\sin(\pi f T)}{\pi f T} e^{-\pi f T}.$$
 (5)

Define V(f) as the transmitter voltage response (TVR). V(f) is not a constant due to imperfect circuit matching to the transducer across the whole signal band. In practice, a precompensation filter could be applied to render V(f) to be close to a constant. Due to a nonideal TVR, the signal x(t) emitted from the transmitter has a Fourier transform of

$$X(f) = V(f)\tilde{S}(f) = V(f)\sum_{k \in \mathcal{S}_A} s[k]G(f - f_k).$$
 (6)

Therefore, frequency dependent attenuation occurs already before the signal enters the water medium.

B. Frequency-dependent propagation and noise

First, consider a static UWA channel. One can represent the multipath channel in the time-domain as

$$h(\tau) = \sum_{p=1}^{N_p} A_p \gamma_p(\tau - \tau_p), \tag{7}$$

and in the frequency domain as

$$H(f) = \sum_{p=1}^{N_p} A_p e^{-j2\pi f \tau_p} \Gamma_p(f),$$
 (8)

where N_p is the number of paths, A_p is the path amplitude for the pth path, $\Gamma_p(f)$ is the frequency-dependent attenuation pattern for the pth path and $\gamma_p(t)$ is the inverse Fourier transform of $\Gamma_p(f)$. Detailed discussions and illustrations of $\Gamma_p(f)$ and $\gamma_p(t)$ can be found in [2], [3].

Now consider a time-varying channel. Within each OFDM symbol, we assume that A_p remains constant, and that the delay on the pth path can be approximated by

$$\tau_p(t) = \tau_p - a_p t,\tag{9}$$

where a_p is the Doppler scale factor on the pth path [11]. The time-varying channel within one OFDM symbol can then be described by

$$h(\tau;t) = \sum_{p=1}^{N_p} A_p \gamma_p(\tau - \tau_p(t))$$
 (10)

with $\tau_p(t)$ defined in (9).

Passing through the time-varying channel in (10), the received signal in the passband is

$$y(t) = x(\tau) \star h(\tau; t) + n(t)$$

$$= \sum_{p=1}^{N_p} A_p \int x(\tau) \gamma_p((1+a_p)t - \tau - \tau_p) d\tau + n(t),$$

$$(11)$$

where n(t) stands for the ambient noise, which may have a colored spectrum. The Fourier transform of y(t) is

$$Y(f) = \sum_{p=1}^{N_p} \frac{A_p}{1+a_p} e^{-j2\pi \frac{f}{1+a_p}\tau_p} \Gamma_p \left(\frac{f}{1+a_p}\right) X\left(\frac{f}{1+a_p}\right) + N(f),$$

$$(12)$$

where N(f) is the Fourier transform of n(t).

C. Receiver intercarrier interference

For simplicity, assume that no resampling operation is necessary. The receiver in [5] will shift the passband signal to baseband, compensate the Doppler shift by multiplying $e^{-j2\pi\epsilon t}$ to the baseband signal, and then perform the FFT operation. The FFT output z_m at the mth subcarrier is simply

$$z_m = Y(f_m + \epsilon), \quad m = -K/2, \cdots, K/2 - 1.$$
 (13)

Substituting (12) and (6) into (13), we obtain equation (14).

$$z_{m} = \underbrace{\left[\sum_{p=1}^{N_{p}} \frac{A_{p}}{1+a_{p}} e^{-j2\pi \frac{f_{m}+\epsilon}{1+a_{p}}\tau_{p}} \Gamma_{p} \left(\frac{f_{m}+\epsilon}{1+a_{p}}\right) V \left(\frac{f_{m}+\epsilon}{1+a_{p}}\right) G \left(\frac{\epsilon-a_{p}f_{m}}{1+a_{p}}\right)\right] s[m]}_{\text{desired signal}} + \underbrace{\left[\sum_{p=1}^{N_{p}} \frac{A_{p}}{1+a_{p}} e^{-j2\pi \frac{f_{m}+\epsilon}{1+a_{p}}\tau_{p}} \Gamma_{p} \left(\frac{f_{m}+\epsilon}{1+a_{p}}\right) V \left(\frac{f_{m}+\epsilon}{1+a_{p}}\right) \sum_{k \in \mathcal{S}_{A}, k \neq m} G \left(f_{m}-f_{k}+\frac{\epsilon-a_{p}f_{m}}{1+a_{p}}\right) s[k]\right]}_{\text{intercarrier interference}}$$

$$+ \underbrace{N(f_{m}+\epsilon)}_{\text{additive noise}}.$$
(14)

$$z_{m} \approx \Gamma\left(f_{m}\right) V\left(f_{m}\right) \left[\sum_{p=1}^{N_{p}} \frac{A_{p}}{1+a_{p}} e^{-j2\pi \frac{f_{m}+\epsilon}{1+a_{p}}\tau_{p}} G\left(\frac{\epsilon-a_{p}f_{m}}{1+a_{p}}\right)\right] s[m]$$

$$+ \Gamma\left(f_{m}\right) V\left(f_{m}\right) \left[\sum_{p=1}^{N_{p}} \frac{A_{p}}{1+a_{p}} e^{-j2\pi \frac{f_{m}+\epsilon}{1+a_{p}}\tau_{p}} \sum_{k \in \mathcal{S}_{A}, k \neq m} G\left(f_{m}-f_{k}+\frac{\epsilon-a_{p}f_{m}}{1+a_{p}}\right) s[k]\right]$$
intercarrier interference
$$+ \underbrace{N(f_{m}+\epsilon)}_{\text{additive paise}}.$$
(15)

Assume that (i) $\Gamma_p(f)$ is the same for all paths, i.e., $\Gamma_p(f) = \Gamma(f)$, (ii) V(f) and $\Gamma(f)$ are smooth, and (iii) $a_p \ll 1$, $\epsilon \ll f_m$. We can then approximate z_m in (14) by the expression in (15). Clearly, the signal power is frequency dependent, and so is the ICI. In fact, the ICI spectrum follows a similar frequency dependency pattern as the desired signal.

In short, the ICI plus noise at the FFT output is non-white. A receiver that ignores this fact might incur considerable performance loss.

III. THE PROPOSED NOISE-WHITENING APPROACH

The receiver from [5] treats both the ICI term and the noise term in (14) as the effective additive Gaussian noise. It operates on an equivalent model as:

$$z_m = H_m s[m] + v_m, (16)$$

where H_m is the frequency response on the mth subcarrier of the composite channel that includes the TVR and the frequency-dependent propagation effects, and v_m incorporates both the additive noise and the ICI. It was assumed in [5] that v_m is white.

A fraction of the data symbols s[k], $k \in \mathcal{S}_P \subset \mathcal{S}_A$ are pilot symbols, which are used to estimate the channel's frequency response H_m . Once the channel estimate is available, one-tap data demodulation is done per subcarrier.

A. Estimating the ICI-plus-noise spectrum

In this paper, we propose a simple method to estimate the variance $\Phi_{vv}[m] = E\{|v_m|^2\}$ of the ICI-plus-noise across all

subcarriers. We assume that the spectrum can be approximated by a straight line in the logarithmic scale, which is an exponential curve in the linear scale. Specifically, we assume

$$\Phi_{vv}[m] = N_0 10^{\kappa m/10} \tag{17}$$

in the linear domain, or

$$10\log_{10}\left(\Phi_{vv}[m]\right) = 10\log_{10}\left(N_0\right) + \kappa m. \tag{18}$$

in the log domain, where $m=-K/2,\ldots,K/2-1$. The parameter N_0 represents the noise variance at the center frequency, while κ is the energy difference in dB between two neighboring subcarriers. The white noise model is included as a special case with $\kappa=0$.

To estimate the model parameters, we use the measurements on the null subcarriers, which are inserted for each OFDM block for Doppler shift compensation [5]. We here propose two methods.

1) Linear Regression (LR) in Log-Domain: A simple linear regression model in the log-domain can be formulated as

$$\left\{ \hat{N}_{0}, \, \hat{\kappa} \right\}_{LR} =$$

$$\arg \min_{N_{0}, \kappa} \sum_{m \in \mathcal{S}_{N}} \left| 10 \log_{10} |z_{m}|^{2} - \left[10 \log_{10} \left(N_{0} \right) + \kappa m \right] \right|^{2}.$$
(19)

This method is of very low complexity. However, fitting in the log-domain tends to lead to negative bias on N_0 (i.e., underestimating the noise variance), as small values are amplified in the log-domain. A simple remedy is to apply some

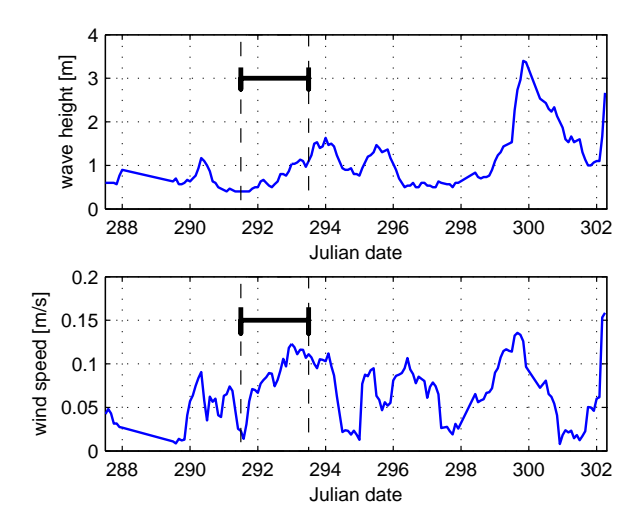


Fig. 1. Wind speed and wave height environmental data of the SPACE08 environment; we consider Julian dates 292 and 293 marked in the figure.

smoothing on the observations $|z_m|^2$ before transforming to the log domain.

2) ML Variance Estimator: By the central limit theorem, v_m can be viewed to have a Gaussian distribution. Hence, $|v_m|^2$ is exponentially distributed. The maximum likelihood (ML) solution for the model parameters can be formulated as

$$\left\{ \hat{N}_{0}, \, \hat{\kappa} \right\}_{\text{ML}} =$$

$$\arg \max_{N_{0}, \kappa} \sum_{m \in \mathcal{S}_{N}} - \left[\log_{10} \left(N_{0} 10^{\kappa m/10} \right) + \frac{|z_{m}|^{2}}{N_{0} 10^{\kappa m/10}} \right].$$

To keep the complexity low, a multi-grid search can be applied or a final solution can be improved via simple interpolation techniques, see e.g., [14].

B. Whitening in the Frequency Domain

Once the variance of the ICI-plus-noise has been estimated, the data can be easily whitened as

$$\tilde{z}_m = \frac{z_m}{\sqrt{\hat{\Phi}_{vv}[m]}} = \tilde{H}_m s[m] + \tilde{v}_m. \tag{21}$$

Channel estimation and data demodulation can then be performed on \tilde{z}_m , where $m \in \mathcal{S}_A$.

IV. EXPERIMENTAL RESULTS

To study the signal and noise power spectrum, we use experimental data from the SPACE08 experiment, which was held off the coast of Martha's Vineyard, Massachusetts, U.S., during October 2008. We will focus on two days of the experiment, namely Julian dates 292 and 293. Fig. 1 shows the wind speed and wave height data for the duration of the experiment, which is helpful for understanding performance differences. We will consider three receivers used in the experiment, as shown in Fig. 2, where receiver S1 was at 60 m from the transmitter, receiver S3 was at 200 m, and receiver S5 was at 1,000 m. Each receiver has multiple phones, which can



Fig. 2. Setup of the receivers S1, S3, and S5 at the SPACE08 experiment.

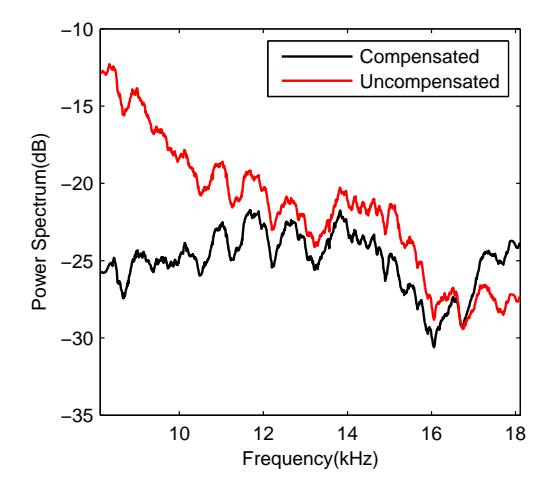


Fig. 3. Measured signal spectrum at the receiver S0, from which we can infer the transmit voltage response. The output power can vary by up to 15 dB across the used frequency band if TVR is not compensated.

be combined to increase effective SNR. An additional receiver S0 was positioned at 1 m from the transmitter.

A. Estimates of Signal Power Spectrum

To estimate the signal power spectrum, we use the FFT outputs on data and pilot subcarriers and evaluate $E\left[|z_m|^2\right]$, $m\in\mathcal{S}_A$, where the expectation is carried out by averaging over a large number of received OFDM blocks. For a time-varying multipath channel, the channel effects could be averaged out, and hence the systematic effects such as the non-ideal TVR and frequency-dependent attenuation can be seen.

The signal spectrum for both the uncompensated and compensated signals on the receiver S0 is shown Fig. 3, from which we can infer the transmit voltage response. Precompensation can reduce the signal power variation across the signal band. However, it leads to a smaller power output in our setting, as the peak-to-average-power control [15] has been applied on the uncompensated signals only; the precompensation filter was not considered during the signal design phase.

Fig. 4 plots the signal spectrum averaged over received data files from Julian Date 292. At receivers S1 and S3, we notice that the compensated signal is approximately white, varying by at most 10 dB across the spectrum. In sharp contrast the uncompensated signal varies by easily 20 dB. The difference matches our estimate of the non-ideal TVR

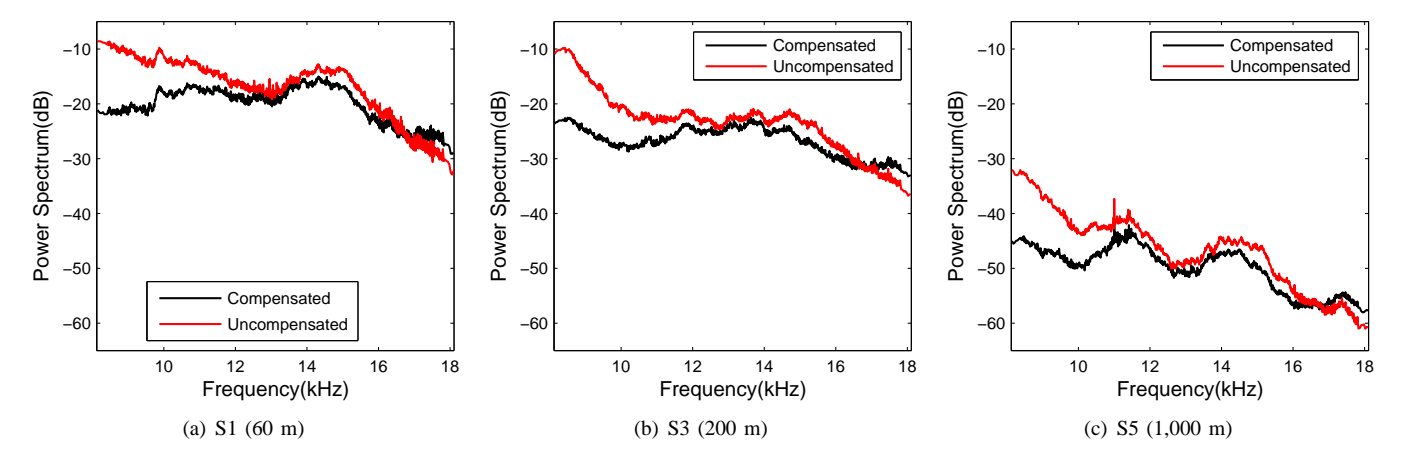


Fig. 4. Experimentally measured signal spectrum at three receivers, Julian Date 292. One can notice the non-ideal TVR in the uncompensated signal. Also the higher frequencies are attenuated more for a long distance.

in Fig. 3. The uncompensated signal has always higher signal power, especially at the lower end of the signal bandwidth. For the receiver S5 at a long distance, the spectrum of the compensated and uncompensated signals have more or less similar overall shapes. Hence, the frequency dependent attenuation has a visible effect at S5.

B. Estimates of Noise Spectrum and Effective SNR

We estimate the ICI-plus-noise spectrum using the proposed linear regression and ML approaches on Julian dates 292 and 293. Comparing the simple linear regression with the ML estimates, we find that the linear regression shows a -3 dB bias in the parameter N_0 as predicted. However, the estimates of the slope parameter κ closely match the ML estimates, as shown in Fig. 5. We observe that the compensated signals at the two closer receivers S1 and S3 have an average slope of $\kappa = 0$, while the uncompensated signals have a significant slope leading to a total difference between the bandwidth edges of $K\kappa \approx 12$ dB. Although the ambient noise should be the same for either signal, the ICI will follow the signal spectrum – in case of the uncompensated signals leading to a significantly colored noise plus ICI spectrum. This points toward the fact that at a close distance from the transmitter, the ICI is dominating the ambient noise. At receiver S5, both signal spectrums are increasingly affected by the frequency dependent attenuation, leading to a colored ICI spectrum. Still, the slope of the uncompensated signals is always about 6 dB more pronounced than that of the compensated signals.

We plot the average received power in Fig. 6, where the x-axis is time, as we average across one receive file at a time, for Julian Dates 292 and 293 to show temporal variation (twenty-four files total), c.f. also Fig. 1. Similar to our previous observations of the signal spectrum, the compensated signals have always about 6 dB less average signal power than the uncompensated signals.

Based on the noise estimates, we plot the estimated effective SNR in Fig. 7, which is the energy ratio of the pilot subcarriers to the null subcarriers. An interesting observation is that although the received signal power decreases from S1 to S3, the effective SNR does not. This again points to the fact that the effective SNR at short range is not limited by noise, but by ICI.

C. BLER Performance

As a further comparison, we look at receiver performance in terms of block-error-rate (BLER). Each OFDM packet has K=1024 subcarriers, consisting of $|\mathcal{S}_N|=96$ null subcarriers and $|\mathcal{S}_P|=256$ pilot subcarriers, leaving $|\mathcal{S}_A|-|\mathcal{S}_P|=672$ for data transmission. We consider 16-QAM constellation, and the rate 1/2 non-binary low density parity check (LDPC) code as in [15]. The symbol duration is T=104.86 ms, the guard time is $T_g=24.6$ ms, leading to a bandwidth of B=K/T=9.77 kHz. This leads to the following spectral efficiency and data rate:

$$\alpha = \frac{T}{T + T_g} \cdot \frac{672}{1024} \cdot \frac{1}{2} \cdot \log_2(16) = 1.06 \text{ bits/s/Hz}, \quad (22)$$

$$R = \alpha B = 10.4 \text{ kb/s.} \tag{23}$$

Two types of channel estimators are used: least-squares (LS) [5] and basis-pursuit (BP) [11].

It is important to note that the min-sum channel decoder used for non-binary LDPC codes [15] does not require a noise variance estimate. Although the linear regression method in (19) does not give a reliable estimate on N_0 , it leads to the same BLER performance as the ML method in (20), as both can estimate the slope κ well and prewhiten the signals in the same fashion; different scalings on the signals do not affect the decoding performance.

The BLER results are plotted in Figs. 8 and 9. We notice that at receivers S1 and S3 – for the compensated signal – the performance assuming white noise is basically identical to that using the ML noise estimates. This is in sharp contrast to the uncompensated signal, which suffers significant performance degradation when not accounting for the colored noise.

As we had seen in Fig. 7, although the uncompensated signal has higher signal power, the effective SNR for the

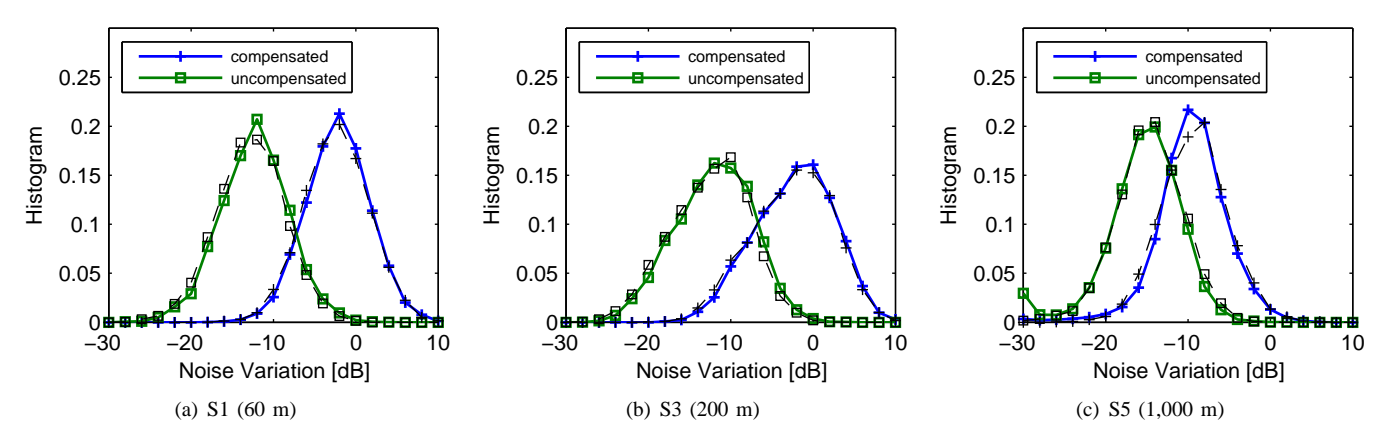


Fig. 5. Histogram of the ML estimates of the noise power difference on subcarriers at the bandwidth edges: $K\kappa$ (also included are the linear regression estimates as black, dashed lines). The compensated signal has a slope around zero for receivers S1 and S3, the uncompensated signal has a significantly colored noise plus ICI spectrum with about 12 dB variation; at S5 both signals have significant variation in the noise spectrum.

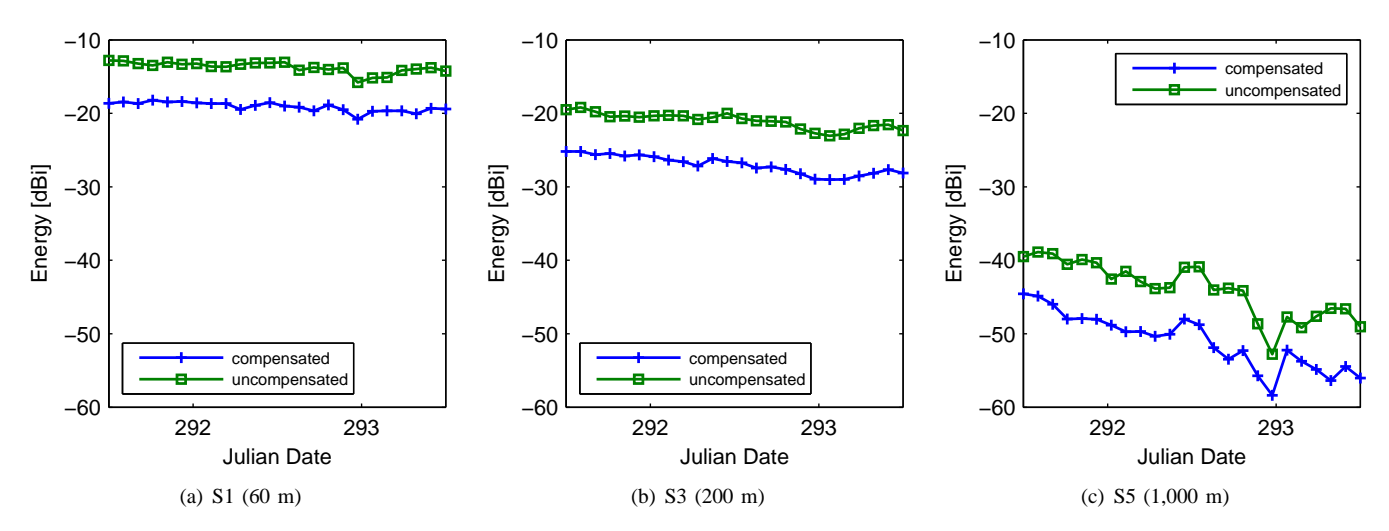


Fig. 6. Experimentally measured average received energy plotted across a time axis for two days of the SPACE08 experiment.

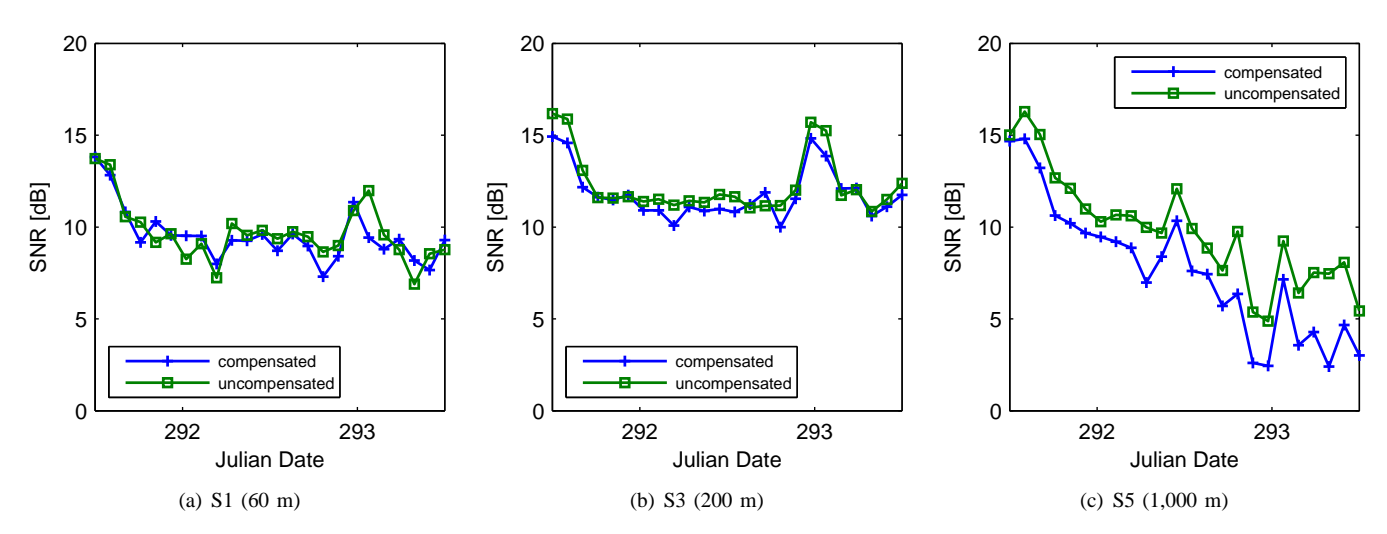


Fig. 7. Experimentally measured effective SNR using the ML estimates of the colored noise spectrum.

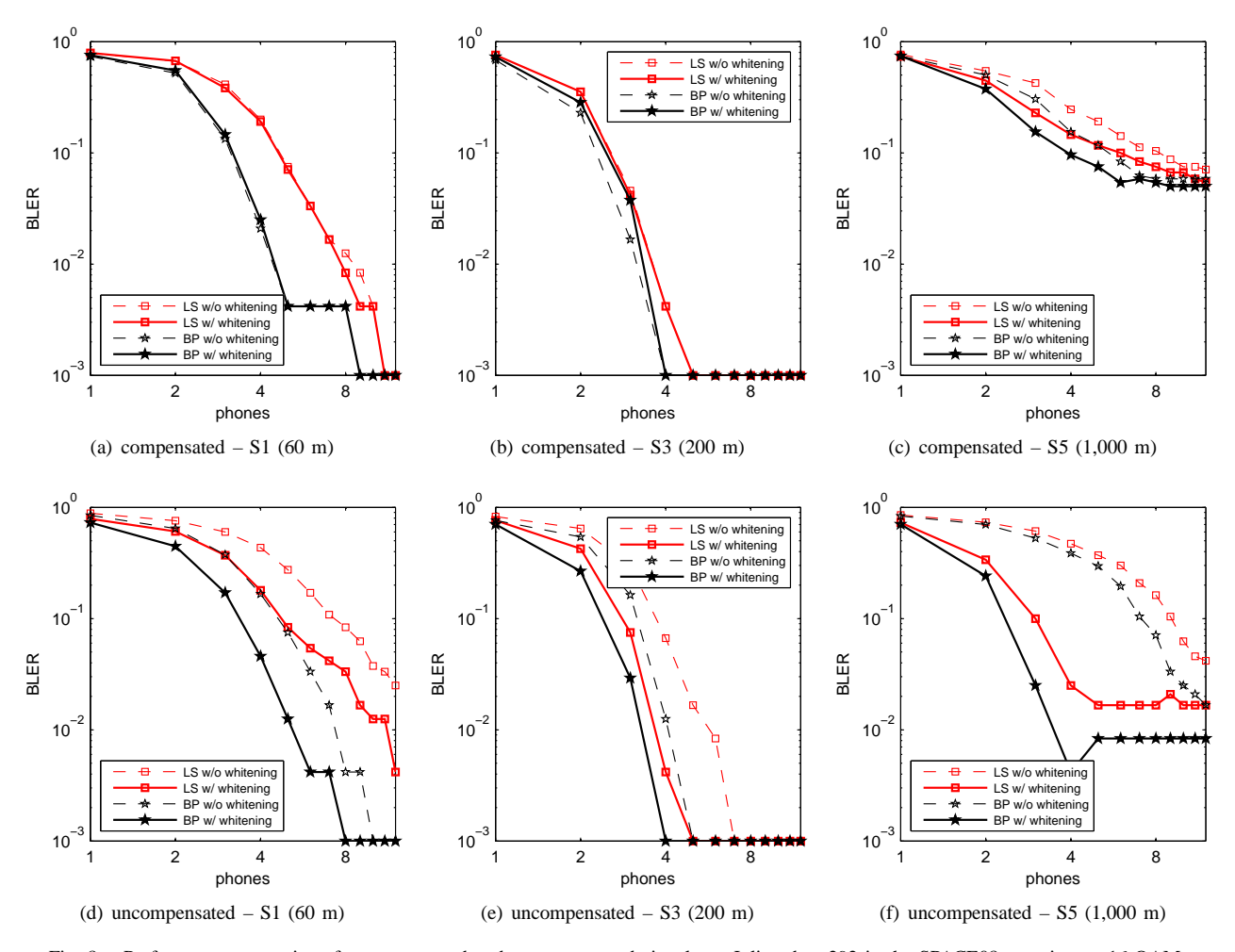


Fig. 8. Performance comparison for compensated and uncompensated signals on Julian date 292 in the SPACE08 experiment, 16-QAM.

compensated and uncompensated signal was virtually the same at S1 and S3. When the colored noise spectrum is accounted for, both signals have approximately the same performance.

At the farthest receiver S5, both signals show improved performance when using the colored noise model. This matches the observation that also the compensated signal has significant noise variation at S5 (c.f. Fig. 5(c)). Furthermore, the uncompensated signals outperform the compensated signals significantly after addressing the colored noise correctly, due to higher transmit power.

V. CONCLUSION

We proposed a simple method to prewhiten the residual inter-carrier-interference (ICI) plus the ambient noise for a block-by-block OFDM receiver, where the noise spectrum is estimated based on observations on the null subcarriers. We tested the performance using two signal sets from the SPACE08 experiment, with or without precompensation on the nonideal transmit voltage response. We find the following:

 At a short transmission distance (60 m, 200 m), the ICI-plus-noise spectrum of the compensated signals is approximately white, but colored for the uncompensated signals. The performance for the uncompensated signals is much worse than that of the compensated ones if noise whitening is not applied, but catches up when noise whitening is applied.

- At a long distance (1,000 m), both the compensated and the uncompensated signals have significantly colored noise. After noise whitening, the uncompensated signals perform even better than the compensated ones due to a higher transmit power level.
- In general the ICI-plus-noise spectrum follows largely
 the signal spectrum, indicating that ICI is the dominant
 source of noise compared to ambient noise. This is
 also reflected in the measured received power versus the
 effective SNR: while the received power continuously
 decreases with distance, the effective SNR changes only
 slightly.

In future work, we would like to investigate the noise whitening effect on OFDM receivers that explicitly deal with ICI, e.g., [11]–[13].

ACKNOWLEDGEMENT

We thank Dr. James Preisig and his team for conducting the SPACE08 experiment.

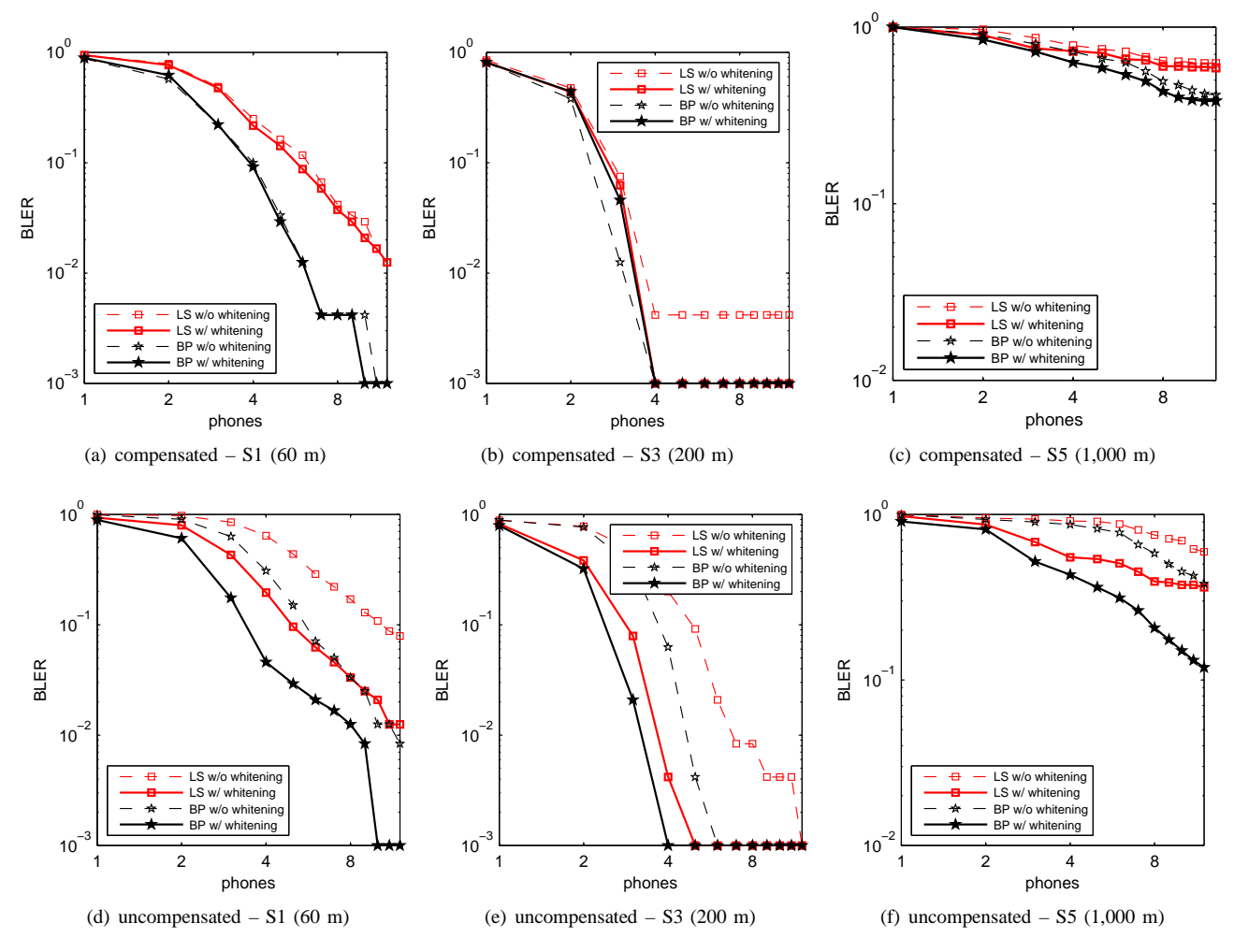


Fig. 9. Performance comparison for compensated and uncompensated signals on Julian date 293 in the SPACE08 experiment, 16-QAM.

REFERENCES

- [1] D. B. Kilfoyle and A. B. Baggeroer, "The state of the art in underwater acoustic telemetry," *IEEE J. Ocean. Eng.*, vol. 25, no. 1, pp. 4–27, Jan. 2000
- [2] M. Stojanovic, "On the relationship between capacity and distance in an underwater acoustic channel," in *Proc. of the ACM Intl. Workshop* on *Underwater Networks (WUWNet)*, Los Angeles, CA, Sept. 2006.
- [3] M. Stojanovic and J. Preisig, "Underwater acoustic communication channels: Propagation models and statistical characterization," *IEEE Communications Magazine*, vol. 47, no. 1, pp. 84–89, Jan. 2009.
- [4] M. Stojanovic, "Low complexity OFDM detector for underwater channels," in *Proc. of MTS/IEEE OCEANS Conf.*, Boston, MA, Sept. 18-21, 2006
- [5] B. Li, S. Zhou, M. Stojanovic, L. Freitag, and P. Willett, "Multicarrier communication over underwater acoustic channels with nonuniform Doppler shifts," *IEEE J. Ocean. Eng.*, vol. 33, no. 2, Apr. 2008.
- [6] M. Stojanovic, "Underwater acoustic communications: Design considerations on the physical layer," in *Proc. of. Conf. on Wireless on Demand Network Systems and Services*, Garmisch-Partenkirchen, Germany, Jan. 2008
- [7] F. Qu and L. Yang, "Basis expansion model for underwater acoustic channels?" in *Proc. of MTS/IEEE OCEANS Conf.*, Quèbec City, Quèbec, Sept. 2008.
- [8] T. Kang and R. A. Iltis, "Iterative carrier frequency offset and channel estimation for underwater acoustic OFDM systems," *IEEE J. Select. Areas Commun.*, vol. 26, no. 9, pp. 1650–1661, Dec. 2008.

- [9] G. Leus and P. A. van Walree, "Multiband OFDM for covert acoustic communications," *IEEE J. Select. Areas Commun.*, vol. 26, no. 9, pp. 1662–1673, Dec. 2008.
- [10] S.-J. Hwang and P. Schniter, "Efficient multicarrier communication for highly spread underwater acoustic channels," *IEEE J. Select. Areas Commun.*, vol. 26, no. 9, pp. 1674–1683, Dec. 2008.
- [11] C. R. Berger, S. Zhou, J. Preisig, and P. Willett, "Sparse channel estimation for multicarrier underwater acoustic communication: From subspace methods to compressed sensing," in *Proc. of MTS/IEEE OCEANS Conf.*, Bremen, Germany, May 2009.
- [12] S. Mason, C. R. Berger, S. Zhou, K. Ball, L. Freitag, and P. Willett, "Receiver comparisons on an OFDM design for Doppler spread channels," in *Proc. of MTS/IEEE OCEANS Conf.*, Bremen, Germany, May 2009.
- [13] K. Tu, D. Fertonani, T. M. Duman, and P. Hursky, "Mitigation of intercarrier interference in OFDM systems over underwater acoustic channels," in *Proc. of MTS/IEEE OCEANS Conf.*, Bremen, Germany, May 2009.
- [14] S. Mason, C. R. Berger, S. Zhou, and P. Willett, "Detection, synchronization, and Doppler scale estimation with multicarrier waveforms in underwater acoustic communication," *IEEE J. Select. Areas Commun.*, vol. 26, no. 9, Dec. 2008.
- [15] J. Huang, S. Zhou, and P. Willett, "Nonbinary LDPC coding for multicarrier underwater acoustic communication," *IEEE J. Select. Areas Commun.*, vol. 26, no. 9, pp. 1684–1696, Dec. 2008.